

Formation of power law spectra of energetic electrons during multiple X line magnetic reconnection with a guide field

Quanming Lu, Huanyu Wang, Kai Huang, Rongsheng Wang, and Shui Wang

Citation: [Physics of Plasmas](#) **25**, 072126 (2018); doi: 10.1063/1.5034012

View online: <https://doi.org/10.1063/1.5034012>

View Table of Contents: <http://aip.scitation.org/toc/php/25/7>

Published by the [American Institute of Physics](#)

PHYSICS TODAY

WHITEPAPERS

MANAGER'S GUIDE

Accelerate R&D with
Multiphysics Simulation

READ NOW

PRESENTED BY

 **COMSOL**

Formation of power law spectra of energetic electrons during multiple X line magnetic reconnection with a guide field

Quanming Lu,^{a)} Huanyu Wang, Kai Huang, Rongsheng Wang, and Shui Wang
 CAS Key Lab of Geospace Environment, School of Earth and Space Sciences, University of Science and Technology of China, Hefei 230026, China

(Received 8 April 2018; accepted 10 July 2018; published online 26 July 2018)

In this paper, with a two-dimensional particle-in-cell simulation model, we study the formation of power-law spectra of energetic electrons in multiple X line magnetic reconnection with a strong guide field. The processes of both magnetic reconnection and electron acceleration can be separated into two stages. In the first stage, two X lines appear at the border and center of the simulation domain, and then, two magnetic islands are formed. In this stage, electrons are accelerated mainly by parallel electric fields, and a power-law spectrum of energetic electrons is generated with the appearance of the second X line. In the second stage, the two magnetic islands are merged into one big island. Besides parallel electric fields, the Fermi mechanism also plays an important role in the production of energetic electrons, and its contribution is comparable to that of parallel electric fields when the electron energy is sufficiently large. In this stage, the generated power-law spectrum of energetic electrons becomes hard. In general, the acceleration efficiencies by both the parallel electric fields and Fermi mechanism become higher with the increase in electron energy, and the tendency is more obvious for the Fermi mechanism. Therefore, both the parallel electric fields and Fermi mechanism are important in the formation of power-law spectra of energetic electrons during multiple X line reconnection. We also investigate the influences of the ion-electron temperature ratio, guide field, and initial flux perturbation on the formed power-law spectra of energetic electrons. *Published by AIP Publishing.* <https://doi.org/10.1063/1.5034012>

I. INTRODUCTION

Energetic electrons associated with explosive phenomena in space and laboratory plasmas, such as solar flares,^{1–3} substorms in the Earth's magnetosphere,^{4–6} and interactions between laser-driven plasma bubbles,^{7–11} generally have a power-law distribution. These phenomena are considered to be related to magnetic reconnection, which converts a tremendous amount of magnetic energy into plasma kinetic energy,^{12–15} and magnetic reconnection provides a critical site to produce energetic electrons. Much previous work has been devoted to revealing physical mechanisms to accelerate electrons during magnetic reconnection. Electrons can be accelerated in the vicinity of the X line by the reconnection electric field,^{16–20} the separatrix region by parallel electric fields,^{20–22} the contracting sites of magnetic island by the Fermi mechanism,^{18,23} and the jet front by the betatron mechanism.^{24–28} They can also be accelerated in the merging region during the coalescence of magnetic islands.^{29–32} Recently, with the use of adiabatic theory, the contributions of parallel electric fields and Fermi and betatron mechanisms to electron acceleration during magnetic reconnection are quantitatively analyzed by summing all electrons in the simulation domain.^{33–40} In weak guide field reconnection, electron acceleration is dominated by the Fermi mechanism, while the contribution of the Fermi mechanism to electron acceleration becomes less and less important with the increase in the guide field.^{33,39} The Betatron mechanism is

usually negligible because it is located only around the jet front. When the guide field is sufficiently large, acceleration by parallel electric fields is the dominant driver for electron energization.^{34,39} However, Dahlin *et al.*³⁴ found that energetic electrons diminish rapidly with the increase in the guide field, and they suggested that compared with the Fermi mechanism parallel electric fields are not an efficient driver for energetic electrons during magnetic reconnection due to their weak energy scaling of particle acceleration.

Although mechanisms of electron acceleration have been thoroughly studied, how power law spectra of energetic electrons are formed during magnetic reconnection is still an unsolved problem. Such kinds of power law spectra are generally observed at reconnection sites in the earth's magnetotail with in-situ observations,⁴ as well as in the solar corona, where electron spectra are deduced from hard X-ray emission of flares.⁴¹ Power law spectra of energetic electrons have also been observed in particle-in-cell (PIC) simulations of magnetic reconnection.^{18,37,38} Li *et al.*^{37,38} ascertained that the condition to form power law spectra of energetic electrons is that magnetic reconnection occurs in a low β plasma. By performing PIC simulations of guide field reconnection, in this paper, we first perform two-dimensional (2D) PIC simulations of multiple X line magnetic reconnection with a strong guide field and study the formation of power law spectra of energetic electrons. Then, based on the adiabatic theory, we analyze the contributions of the parallel electric fields and Fermi mechanism to the formation of the power law spectrum of these energetic electrons. The influences of the ion-electron temperature ratio, guide field, and

^{a)} Author to whom correspondence should be addressed: qmlu@ustc.edu.cn

initial flux perturbation on the formed power-law spectra are also investigated.

This paper is organized as follows: In Sec. II, we describe the simulation model. In Sec. III, the simulation results are presented. Finally, conclusions and discussion are given in Sec. IV.

II. SIMULATION MODEL

A 2D PIC simulation model is used in this paper to investigate the formation of the electron energy spectrum during multiple X line reconnection with a guide field. In our PIC simulations, the electromagnetic fields are defined on the grids and updated by solving the Maxwell equation with a full explicit algorithm, and ions and electrons are advanced in these electromagnetic fields. The initial configuration of the magnetic field consists of a uniform guide field superimposed by a Harris equilibrium. The magnetic field and the corresponding number density are given by

$$B_0(z) = B_0 \tanh(z/\delta) \mathbf{e}_x + B_{0y} \mathbf{e}_y, \quad (1)$$

$$n(z) = n_b + n_0 \operatorname{sech}^2(z/\delta), \quad (2)$$

where B_0 is the asymptotic magnetic field, δ is the half-width of the current sheet, B_{0y} is the initial guide field perpendicular to the reconnection plane, n_b is the number density of the background plasma, and n_0 is the peak Harris number density. The initial distribution functions for ions and electrons corresponding to the Harris current sheet are Maxwellian with a drift speed in the y direction, and the drift speeds satisfy the following equation: $V_{i0}/V_{e0} = -T_{i0}/T_{e0}$, where $V_{e0}(V_{i0})$ and $T_{e0}(T_{i0})$ are the initial drift speed and the temperature of electrons (ions), respectively. The initial distributions for ions and electrons corresponding to the background plasma satisfy the Maxwellian function without a bulk velocity, and their initial temperatures are the same as those corresponding to the Harris current sheet. We set the ion-to-electron mass ratio as $m_i/m_e = 100$, and the light speed is $c = 15v_A$ (where v_A is the Alfvén speed based on B_0 and n_0). The computations are carried out in a rectangular domain in the (x, z) plane with the dimension $L_x \times L_z = 60d_i \times 15d_i$. The grid number is $N_x \times N_z = 1200 \times 300$. Therefore, the spatial resolution is $\Delta x = \Delta z = 0.05d_i$. The time step is $\Omega_i t = 0.001$, where $\Omega_i = eB_0/m_i$ is the ion gyrofrequency. We employ 500 particles per cell to represent the peak Harris number density n_0 , and totally more than 10^9 particles per species are used in the simulation. We employ the periodic boundary condition for the electromagnetic field and particles in the x direction, and the ideal conducting boundary condition for the electromagnetic field and the reflected boundary condition for particles in the z direction are used. The reconnection is initiated by small local flux perturbations to trigger multiple X line reconnection.

III. SIMULATION RESULTS

We run a series of 2-D PIC simulations with the variations of the guide field B_{0y} , ion-to-electron temperature ratio T_{i0}/T_{e0} , and the initial flux perturbation to investigate the formation of

power law spectra of energetic electrons during magnetic reconnection with a guide field. At first, we run a benchmark case, where $B_{0y} = 2.0B_0$, $T_{i0}/T_{e0} = 4$, $n_b = 0.2n_0$, and $\delta = 0.5d_i$ (where $d_i = c/\omega_{pi}$ is the ion inertial length defined on n_0), and the reconnection is initiated by small local flux perturbations centered at $x = 30d_i$ and $x = 60d_i$ to trigger multiple X line reconnection with two magnetic islands in the simulation domain. In the following, if there is no explicit statement, we are describing the benchmark case.

The time evolution of magnetic reconnection is shown in Fig. 1, which displays the magnetic field lines and distributions of the number density of energetic electrons with energy larger than $\varepsilon_e > 1.0m_e c^2$ at $\Omega_i t = 25, 30, 40, 43, 70$, and 80. The reconnection of magnetic field lines begins at about $\Omega_i t = 20$, and one X line appears around the border of the simulation domain. At this time, we can only find one magnetic island in the simulation domain. At about $\Omega_i t = 30$, another X line is formed around the center of the simulation domain, and then, two magnetic islands are generated in the simulation domain. The two magnetic islands begin to coalesce at about $\Omega_i t = 43$, and they are merged into a big island at about $\Omega_i t = 80$. The number of energetic electrons increases continuously with the proceeding of multiple X reconnection, including the stages with the appearance and merging of magnetic islands. These energetic electrons are concentrated around the edges of magnetic islands.

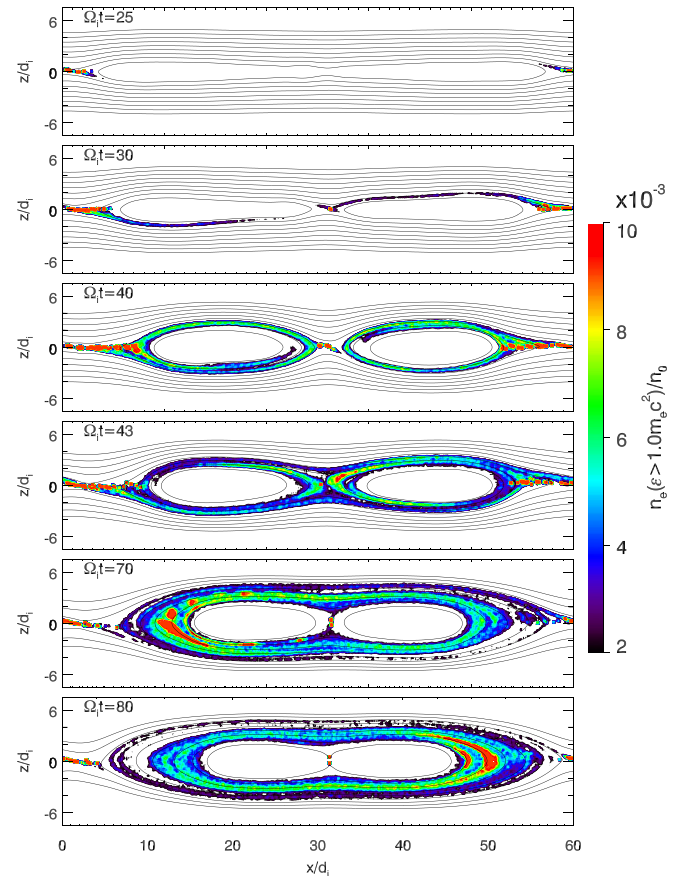


FIG. 1. The time evolution of magnetic field lines and distributions of number density of energetic electrons with energy larger than $\varepsilon_e > 1.0m_e c^2$ at $\Omega_i t = 25, 30, 40, 43, 70$, and 80. The number density of energetic electrons in the simulation domain is normalized by the peak Harris number density n_0 .

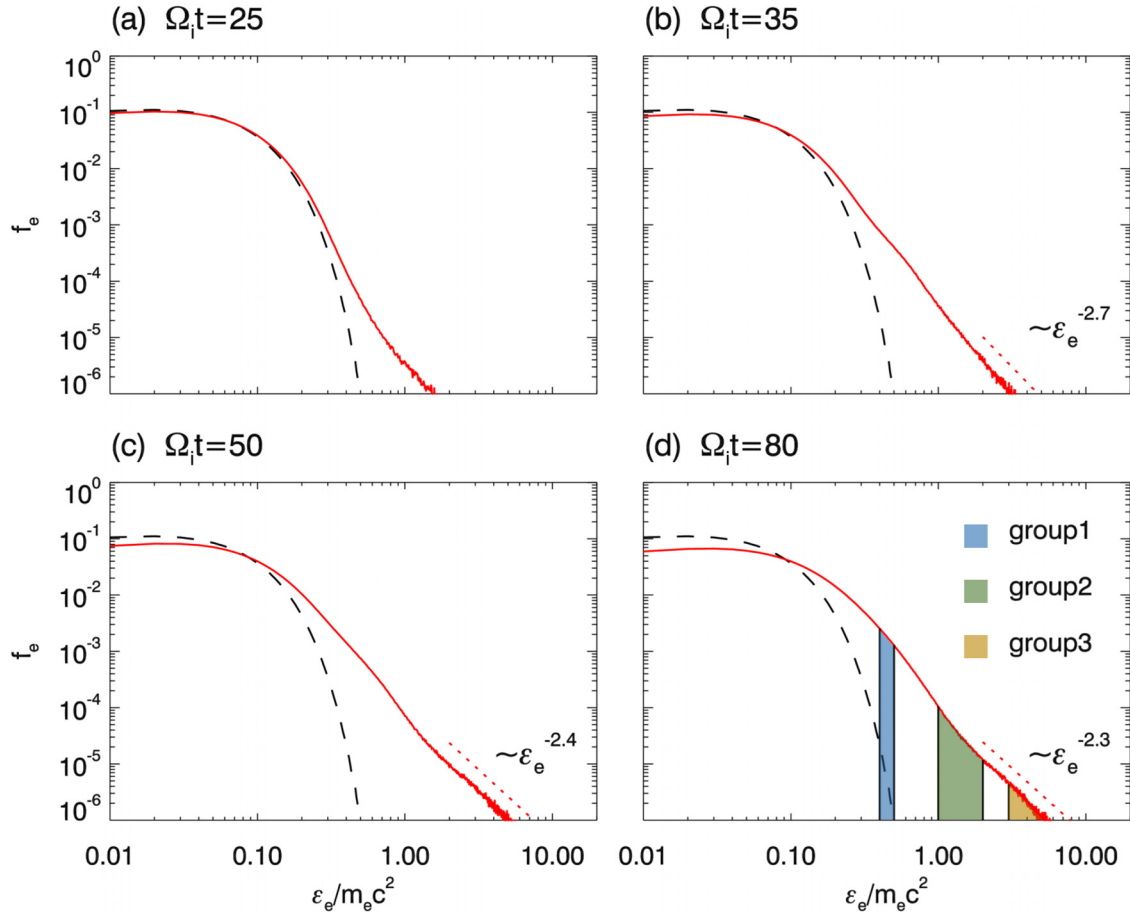


FIG. 2. The electron energy spectra at $\Omega_i t =$ (a) 25, (b) 35, (c) 50, and (d) 80. The black dashed lines are the electron energy spectrum at $\Omega_i t = 0$, the red dashed lines are the fitted Maxwellian distributions at low electron energy, and the dotted line is the fitted power-law distribution at high electron energy. The ranges of electron energy denoted by groups 1, 2, and 3 in (d) are $0.4m_e c^2 < \varepsilon_e < 0.5m_e c^2$, $1.0m_e c^2 < \varepsilon_e < 2.0m_e c^2$, and $\varepsilon_e > 3.0m_e c^2$, respectively.

The process of electron acceleration during multiple X line reconnection can be demonstrated more clearly in Fig. 2, which plots the electron energy spectra at $\Omega_i t =$ (a) 25, (b) 35, (c) 50, and (d) 80. For reference, the electron energy spectrum at $\Omega_i t = 0$ is also shown with black dashed lines, and the red dashed lines are the fitted Maxwellian distributions with low electron energy. Obviously, the electron energy spectra consist of two components: thermal and super-thermal parts. The super-thermal part of electron distribution begins to have a power law spectrum with the appearance of the second magnetic island, which is ubiquitously observed in space plasma.^{42–44} At $\Omega_i t = 35$, the index of power-law distribution is about 2.7, and it becomes hard when the two magnetic islands begin to be merged. The indexes are about 2.4 and 2.3 at $\Omega_i t = 50$ and 80, respectively.

In magnetic reconnection with a strong guide field, the electron motions can be assumed to satisfy the guide-center approximation, and the energy evolution of a single electron can be given as^{33,39,45}

$$\frac{d\varepsilon}{dt} = -eE_{\parallel}v_{\parallel} + \gamma m_e v_{\perp}^2 (\mathbf{u}_E \cdot \boldsymbol{\kappa}) + \frac{\mu}{\gamma} \left(\frac{\partial B}{\partial t} + \mathbf{u}_E \cdot \nabla B \right), \quad (3)$$

where $\mu = m_e \gamma^2 v_{\perp}^2 / 2B$ is the magnetic moment and γ is the Lorentz factor. \mathbf{u}_E is the “ $\mathbf{E} \times \mathbf{B}$ ” drift velocity and $\boldsymbol{\kappa} = \mathbf{b} \cdot \nabla \mathbf{b}$ (where $\mathbf{b} = \mathbf{B}/B$ is the unit vector in the direction

of the local magnetic field) is the curvature of the magnetic field. The first term on the right-hand-side of Eq. (3) is the contribution by parallel electric fields, and the second term drives parallel acceleration, which arises from the first-order Fermi mechanism. The last term is the betatron mechanism corresponding to perpendicular heating or cooling due to the conservation of the magnetic momentum μ . In our simulation, the betatron mechanism is negligible. Therefore, in this paper, we will not consider its contribution to energetic electrons in the following.

In order to know how a power-law distribution of energetic electrons is produced in multiple X lines with a guide field, the contributions by the parallel electric fields and Fermi mechanism at different energies are analyzed. Figure 3 shows the time evolution of the average contributions of the parallel electric fields and Fermi mechanism per particle for electrons with energies (a) $0.4m_e c^2 < \varepsilon_e < 0.5m_e c^2$ [group 1 as denoted in Fig. 2(d)], (b) $1.0m_e c^2 < \varepsilon_e < 2.0m_e c^2$ [group 2 as denoted in Fig. 2(d)], and (c) $\varepsilon_e > 3.0m_e c^2$ [group 3 as denoted in Fig. 2(d)]. It can be found that with the increase in electron energy, the efficiencies of electron acceleration by both the parallel electric fields and Fermi mechanism are enhanced, and the enhancement of the Fermi mechanism is more obvious than that of parallel electric field. The electron acceleration can be roughly separated into two stages. During the first stage

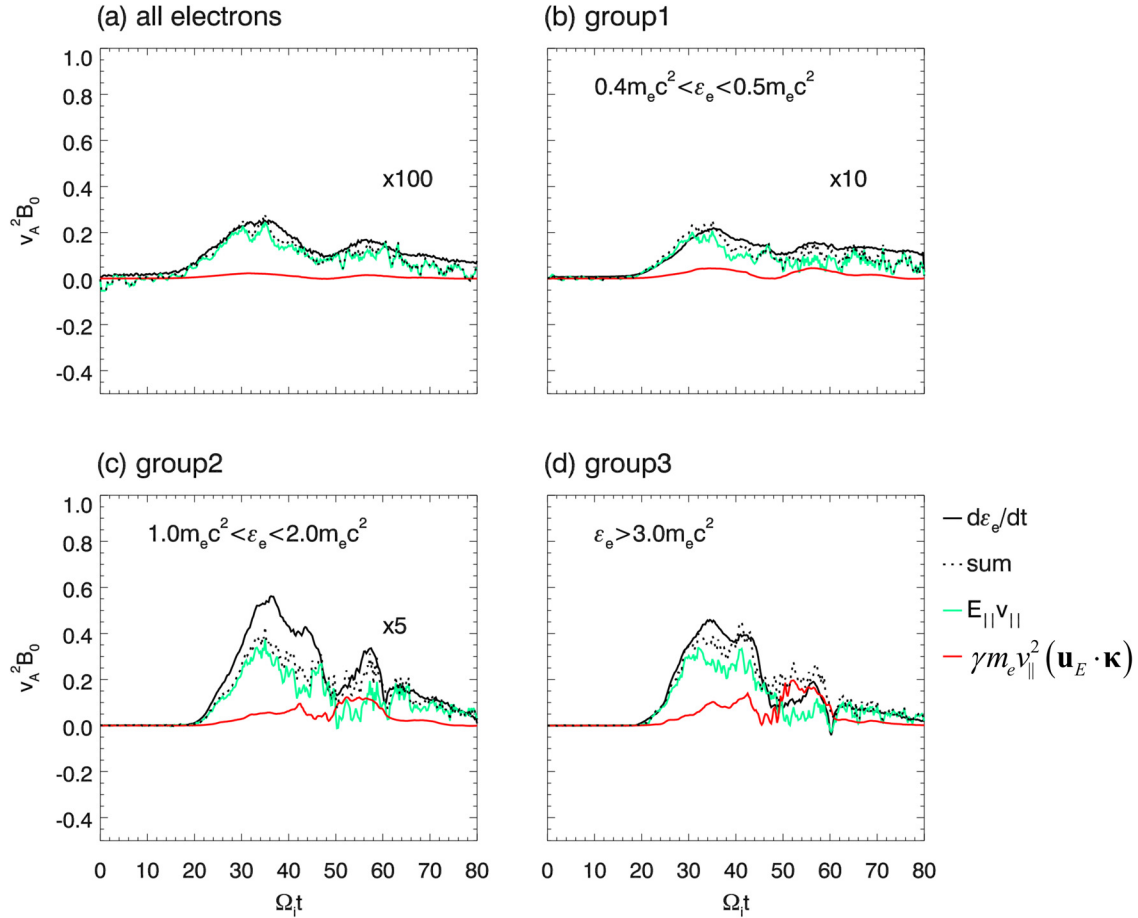


FIG. 3. The time evolution of the average contributions of parallel electric fields and Fermi mechanism per particle for electrons with energies (a) $0.4m_e c^2 < \epsilon_e < 0.5m_e c^2$ [group 1 as denoted in Fig. 2(d)], (b) $1.0m_e c^2 < \epsilon_e < 2.0m_e c^2$ [group 2 as denoted in Fig. 2(d)] and (c) $\epsilon_e > 3.0m_e c^2$ [group 3 as denoted in Fig. 2(d)]. Here, the contributions are normalized by $v_A^2 B_0$.

($\Omega_i t < 43$), two X lines appear at the border and center of the simulation domain, and two magnetic islands are formed. Electrons are accelerated mainly by parallel electric field, and the contribution of the Fermi mechanism is very small. During the second stage ($\Omega_i t > 43$), the two islands are merged into a big island, and the contribution of the Fermi mechanism becomes more and more important with the increase of electron energy, compared with that of parallel electric fields. For these electrons with energy larger than

$3.0m_e c^2$, the contribution of the Fermi mechanism is comparable to that of parallel electric field.

The relative importance of the parallel electric field and Fermi mechanism in the two stages can be quantitatively estimated by integrating their contributions to electron acceleration in the first and second stages, respectively. Figure 4 plots the percentages of the contributions of parallel electric fields and Fermi mechanism to the sum of all contributions (including parallel electric fields, Fermi and betatron mechanisms)

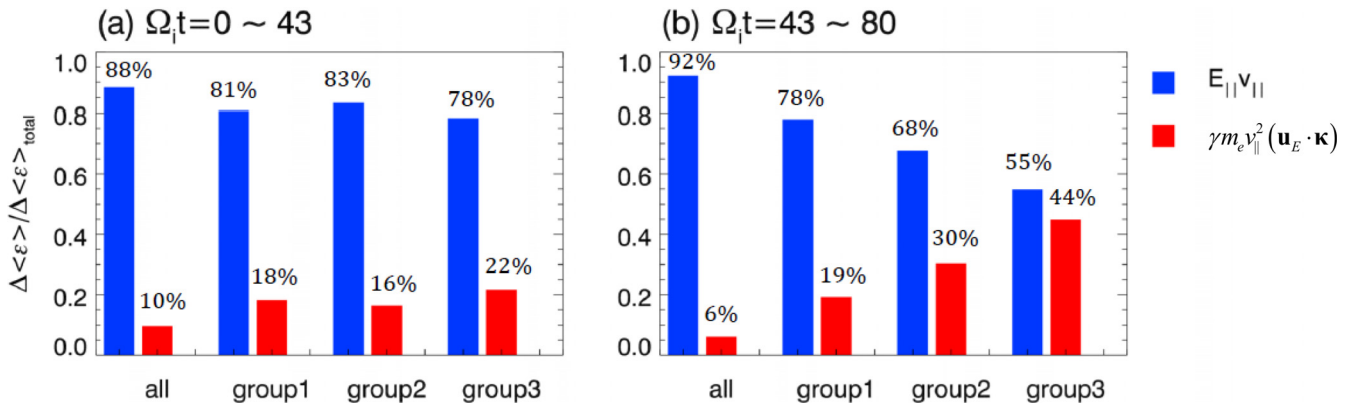


FIG. 4. The percentages of the contributions of parallel electric fields and Fermi mechanism to the sum of all contributions (including parallel electric fields, Fermi and betatron mechanisms) during (a) the first stage ($\Omega_i t < 43$) and (b) the second stage ($43 < \Omega_i t < 80$).

mechanisms) during (a) the first stage ($\Omega_i t < 43$) and (b) the second stage ($43 < \Omega_i t < 80$). In the first stage, the electrons are mainly accelerated by parallel electric field, and the percentages of the contribution of the Fermi mechanism are 18%, 16%, and 22% for electrons with energy $0.4m_e c^2 < \varepsilon_e < 0.5m_e c^2$, $1.0m_e c^2 < \varepsilon_e < 2.0m_e c^2$, and $\varepsilon_e > 3.0m_e c^2$, respectively. In the second stage, the percentages of the contribution of the Fermi mechanism are 19%, 30%, and 44% for electrons with energy $0.4m_e c^2 < \varepsilon_e < 0.5m_e c^2$, $1.0m_e c^2 < \varepsilon_e < 2.0m_e c^2$, and $\varepsilon_e > 3.0m_e c^2$, respectively. Therefore, the contribution of the Fermi mechanism is comparable to that of parallel electric field when electron energy is sufficiently large.

Figures 5 and 6 plot two typical electron trajectories, which belong to group 1 and 3, respectively. During the first stage, the acceleration of both the electrons is mainly attributed to parallel electric fields. The electron belonging to group 3 can also be accelerated by the Fermi mechanism,

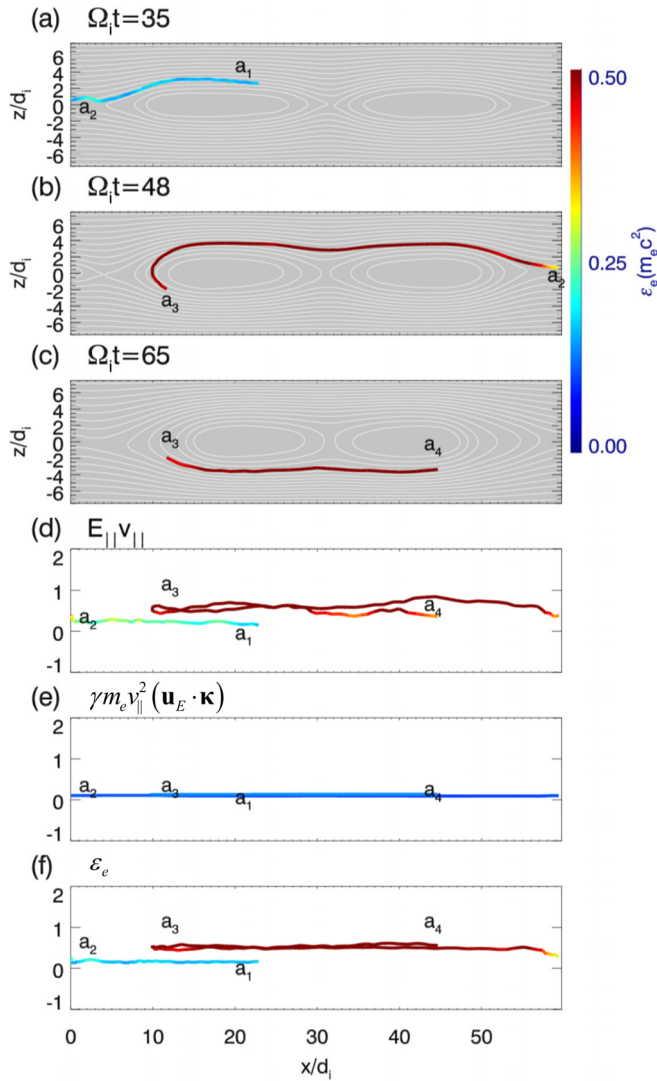


FIG. 5. A typical electron trajectory, which belongs to group 1. (a), (b), and (c) are the trajectory and energy evolution from $a_1(\Omega_i t = 30)$ to $a_2(\Omega_i t = 45)$, a_2 to $a_3(\Omega_i t = 60)$, and a_3 to $a_4(\Omega_i t = 70)$, respectively. For reference, the magnetic field lines at $\Omega_i t = 35$, 48, and 65 are plotted in (a), (b), and (c). (d) and (e) are the obtained energy accelerated by the parallel electric field and Fermi mechanism, and (f) is the sum.

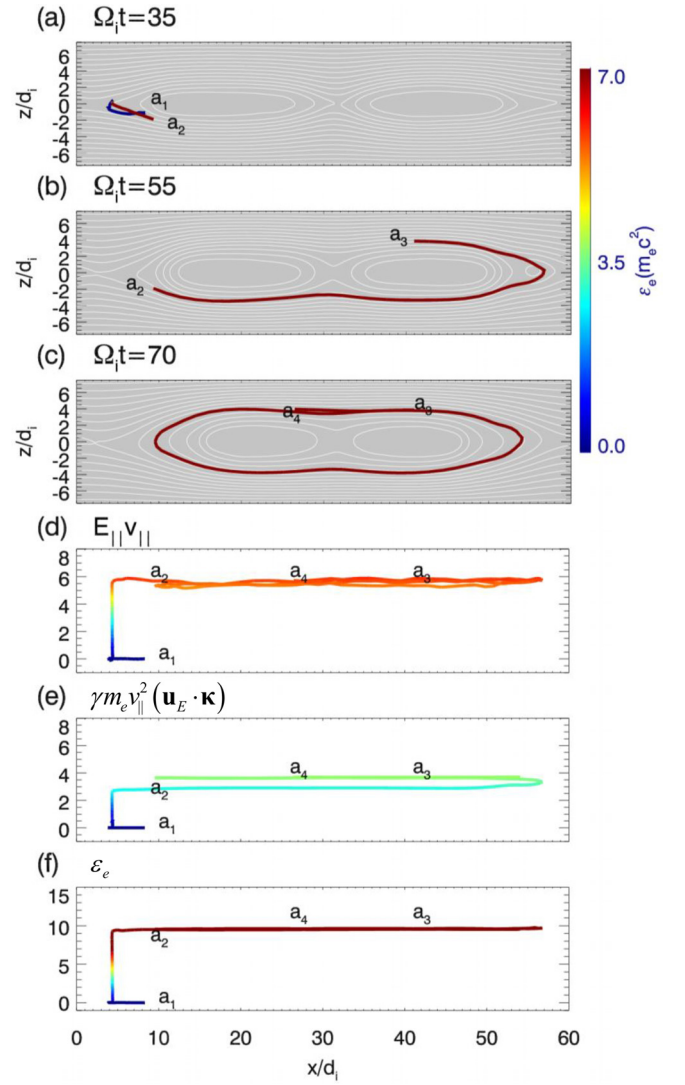


FIG. 6. A typical electron trajectory, which belongs to group 3. (a), (b), and (c) are the trajectory and energy evolution from $a_1(\Omega_i t = 15)$ to $a_2(\Omega_i t = 48.75)$, a_2 to $a_3(\Omega_i t = 60)$, and a_3 to $a_4(\Omega_i t = 80)$, respectively. For reference, the magnetic field lines at $\Omega_i t = 35$, 55 and 70 are plotted in (a), (b), and (c). (d) and (e) are the obtained energy accelerated by the parallel electric field and Fermi mechanism, and (f) is the sum.

while the Fermi mechanism is negligible for the electron belonging group 1. The electron belonging to group 3 obtains much higher energy in the first stage. During the second stage, both the electrons can be further accelerated. However, the electron belonging to group 1 is mainly accelerated by parallel electric fields, while for the electron belonging to group 3 both the parallel electric fields and Fermi mechanism are important for its acceleration. Finally, the electron belonging to group 3 has much higher energy after the two-stage acceleration.

Figure 7 shows the electron energy spectra at $\Omega_i t = 80$ for the different ion-to-electron temperature ratio (a) $T_{i0}/T_{e0} = 1$ and (b) $T_{i0}/T_{e0} = 1/3$ while all other parameters are kept as those in the benchmark case. We find that the variation of the ion-to-electron temperature ratio almost does not change the evolution of magnetic field lines with the proceeding of magnetic reconnection (not shown). The electron energy spectra can also be considered to a superposition of

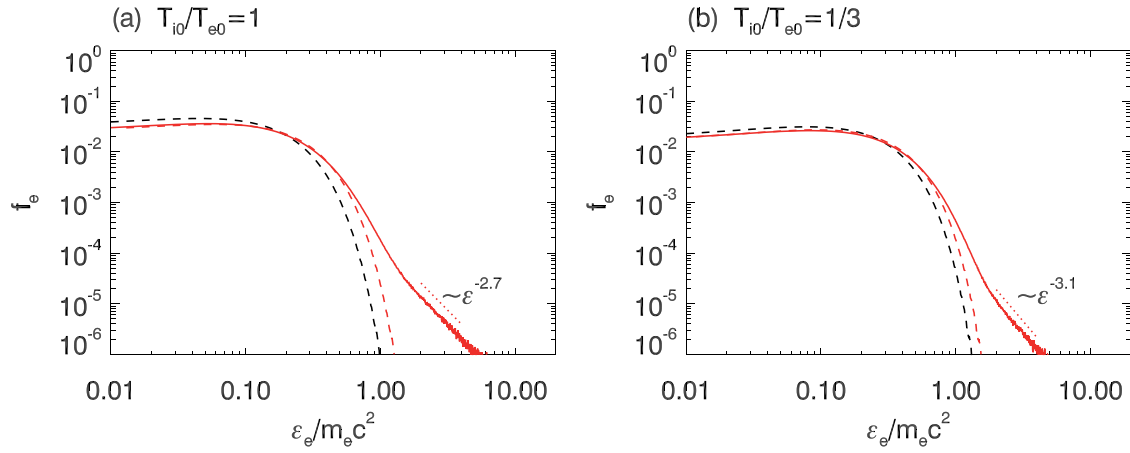


FIG. 7. The electron energy spectra at $\Omega_i t = 80$ for the different ion-to-electron temperature ratio (a) $T_{i0}/T_{e0} = 1$ and (b) $T_{i0}/T_{e0} = 1/3$ while all other parameters are kept as those in the benchmark case.

the Maxwellian function at the lower energy and power law spectrum at higher energy. However, with the decrease in the ion-to-electron temperature ratio the electrons are hard to be accelerated and to form a tail with a power law spectrum. The indexes of the power law spectra at $\Omega_i t = 80$ for the different ion-to-electron temperature ratio $T_{i0}/T_{e0} = 1$ and $T_{i0}/T_{e0} = 1/3$ are about 2.7 and 3.1, respectively.

Figure 8 plots the electron energy spectra at $\Omega_i t = 80$ for the different guide field (a) $B_{0y} = 1.0B_0$ and (b) $B_{0y} = 0.5B_0$ while all other parameters are kept as those in the benchmark case. The variation of the guide field also changes little the evolution of magnetic field lines during magnetic reconnection (not shown), and with a decrease in the guide field the electrons are hard to form a high-energy tail with a power law spectrum, and the indexes of the power law spectra at $\Omega_i t = 80$ for $B_{0y} = 1.0B_0$ and (b) $B_{0y} = 0.5B_0$ are about 2.4 and 3.2, respectively.

We also investigate the influence of the initial flux perturbation on the formation of power law spectra of energetic electrons. Figure 9 shows the time evolution of the magnetic field lines and distributions of the number density of energetic electrons with energy larger than $\epsilon_e > 1.0m_e c^2$ at $\Omega_i t = 30, 40, 80, 100,$ and 150 . Compared with the benchmark case, at first four magnetic islands are formed. At about

$\Omega_i t = 40$, these islands begin to coalesce. There exist three and two islands at about $\Omega_i t = 50$ and 70 , respectively. At last, only one island remains at about $\Omega_i t = 130$. Figure 10 plots the electron energy spectra at $\Omega_i t = 150$. The energetic electrons still have a power law spectrum with the index about 1.9, which is smaller than that of the benchmark case.

IV. CONCLUSIONS AND DISCUSSION

Satellite observations have shown that energetic electrons associated with explosive phenomena, such as solar flare and substorm in the earth's magnetotail, generally have power-law spectra, and these energetic electrons are considered to be generated during magnetic reconnection. However, how power-law spectra of energetic electrons are formed during magnetic reconnection is still a puzzle. In this paper, by performing 2-D PIC simulations, the generation of power-law spectra of energetic electrons in multiple X line reconnection with a strong guide field is analyzed in detail by assuming that electron motions satisfy the guide-center approximation. In the benchmark case, a power-law spectrum of energetic electrons is formed with the appearance of two X lines in the simulation domain (also two magnetic islands), and the electrons are mainly accelerated by parallel

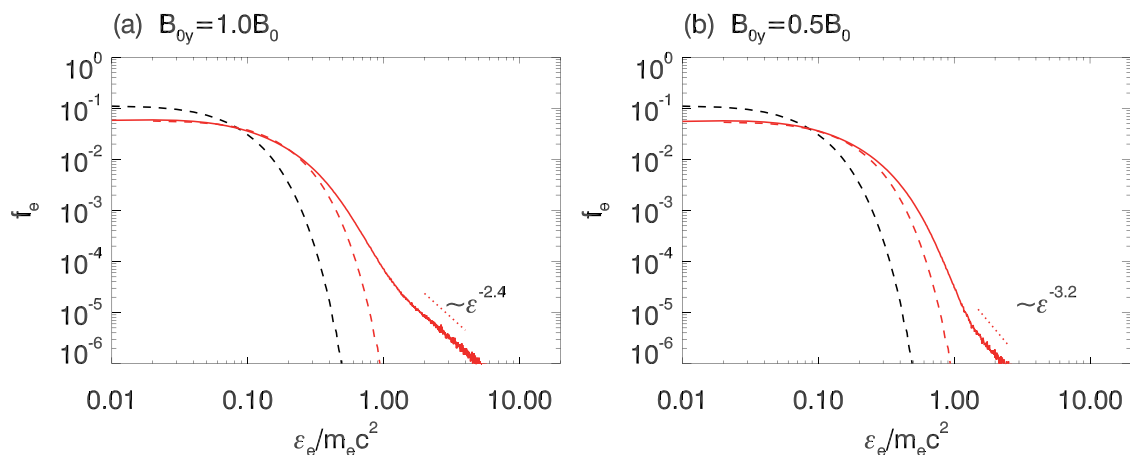


FIG. 8. The electron energy spectra at $\Omega_i t = 80$ for the different guide field (a) $B_{0y} = 1.0B_0$ and (b) $B_{0y} = 0.5B_0$ while all other parameters are kept as those in the benchmark case.

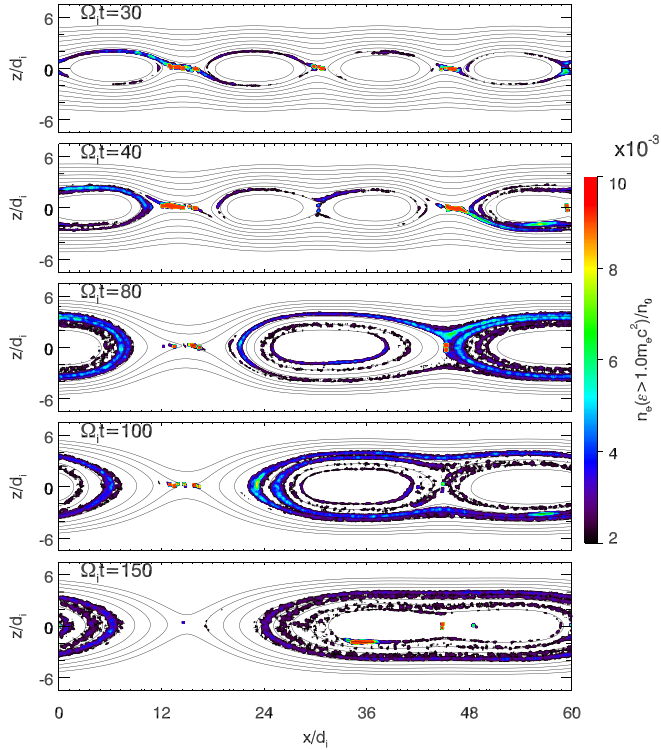


FIG. 9. The magnetic field lines and distributions of the number density of energetic electrons with energy larger than $\varepsilon_e > 1.0m_e c^2$ at $\Omega t = 30, 40, 80, 100$, and 150 . Compared with the benchmark case, here we use a different flux perturbation and at first four magnetic islands are formed.

electric fields. The electrons can be further accelerated when the two magnetic islands are merged into one big island by both the parallel electric fields and Fermi mechanism, and their spectrum becomes hard. In our simulation, we also find that with the increase of electron energy the acceleration efficiencies of both the parallel electric field and Fermi mechanism tend to be higher, and the tendency is more obvious for the Fermi mechanism. It is not strange, because acceleration by the parallel electric fields and Fermi mechanism scales with $\varepsilon^{1/2}$ (where ε is particle energy) and ε , respectively.³⁴ In

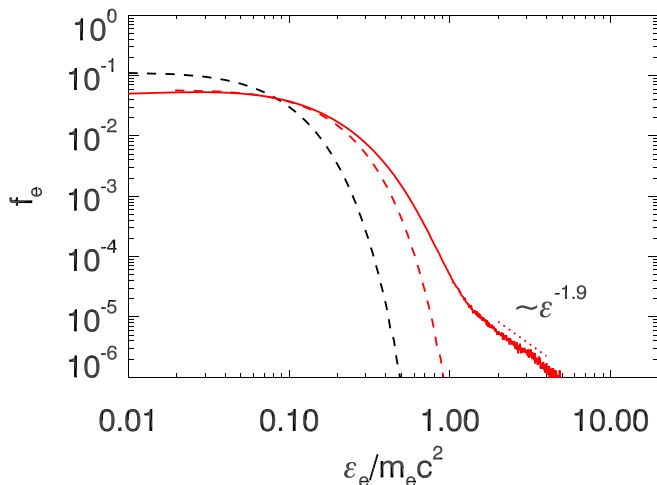


FIG. 10. The electron energy spectra at $\Omega t = 150$. Compared with the benchmark case, here we use a different flux perturbation and at first four magnetic islands are formed.

multiple X line magnetic reconnection, electrons are first accelerated by parallel electric fields around the X line with the generation of magnetic islands and get a large energy. During the coalescence of magnetic islands, the electrons are further accelerated by the parallel electric fields and Fermi mechanism. Because the Fermi mechanism scales more strongly with the particle energy than parallel electric fields, it will play a more important role in the generation of higher energy electrons and then formation of a power-law spectrum.

Also note because we use a periodic boundary condition in our simulations, it implies that the current sheet is sufficiently long to accommodate many islands, which can interact with each other. In reality, the generated current sheet in space plasma is usually sufficiently long to trigger multiple X line magnetic reconnection and many islands can be formed. Our simulations have demonstrated that the produced energetic electrons in such a situation can have a power-law spectrum. Therefore, our simulation provides an explanation for the power-law spectra of energetic electrons, which is ubiquitously observed in explosive phenomena.

We also investigate the effects of the ion-to-electron temperature ratio, guide field, and initial flux perturbation on power law spectra of energetic electrons formed during multiple X line reconnection. The decrease in the ion-to-electron temperature ratio will lead to the softening of the formed power law spectrum, and the increase in the guide field will make the high energy tail have a hard power law spectrum. The initial flux perturbation will also change the formed power law spectrum of energetic electrons during multiple X line reconnection. The power law spectra of energetic electrons are easy to be formed during multiple X line reconnection. This is different from Li *et al.*,³⁷ where a force free current sheet is used and a power law spectrum of energetic electrons can only be formed in a low plasma β regime. Dahlin *et al.*^{33,34} found that energetic electrons are hard to be formed in a power law spectrum during magnetic reconnection during either a Harris or force free current. It seems that a contradictory conclusion is obtained among these simulations, and further studies are necessary to resolve this discrepancy.

ACKNOWLEDGMENTS

We thank Dr. C. Huang for fruitful discussion with Dr. C. Huang. This work was supported by the NSFC Grant Nos. 41474125, 41331067, 41774169, and 41527804, Key Research Program of Frontier Sciences, CAS (QYZDJ-SSW-DQC010), and the Fundamental Research Funds for the Central Universities.

¹R. P. Lin and H. S. Hudson, *Sol. Phys.* **50**, 153 (1976).

²J. A. Miller, P. J. Cargill, A. Emslie, G. D. Holman, B. R. Dennis, T. N. Larosa, R. M. Winglee, S. G. Benka, and S. Tsuneta, *J. Geophys. Res.* **102**, 14631, <https://doi.org/10.1029/97JA00976> (1997).

³R. P. Lin, S. Krucker, G. J. Hurford, D. M. Smith, H. S. Hudson, G. D. Holman, R. A. Schwartz, B. R. Dennis, G. H. Share, and R. J. Murphy, *Astrophys. J. Lett.* **595**, L69 (2003).

⁴M. Øieroset, R. P. Lin, T. D. Phan, D. E. Larson, and S. D. Bale, *Phys. Rev. Lett.* **89**, 195001 (2002).

- ⁵S. Imada, R. Nakamura, P. W. Daly, M. Hoshino, W. Baumjohann, S. Mühlbacher, A. Balogh, and H. Rème, *J. Geophys. Res.* **112**, A03202, <http://doi.org/10.2019/2006JA011847> (2007).
- ⁶R. S. Wang, Q. M. Lu, C. Huang, and S. Wang, *J. Geophys. Res.* **115**, A01209, <http://doi.org/10.1029/2009JA014553> (2010).
- ⁷Q. L. Dong, S. J. Wang, Q. M. Lu, C. Huang, D. W. Yuan, X. Liu, X. X. Lin, Y. Li, H. G. Wei, J. Y. Zhong, J. R. Shi, S. E. Jiang, Y. K. Ding, B. B. Jiang, K. Du, X. T. He, M. Y. Yu, C. S. Liu, S. Wang, Y. J. Tang, J. Q. Zhu, G. Zhao, Z. M. Sheng, and J. Zhang, *Phys. Rev. Lett.* **108**, 215001 (2012).
- ⁸S. Lu, Q. M. Lu, F. Guo, Z. M. Sheng, H. Y. Wang, and S. Wang, *New J. Phys.* **18**, 013051 (2016).
- ⁹S. R. Titorica, T. Abel, and F. Fiuza, *Phys. Rev. Lett.* **116**, 095003 (2016).
- ¹⁰W. Fox, J. Park, W. Deng, G. Fiksel, A. Spitkovsky, and A. Bhattacharjee, *Phys. Plasmas* **24**, 092901 (2017).
- ¹¹K. Huang, Q. M. Lu, C. Huang, Q. L. Dong, H. Y. Wang, F. B. Fan, Z. M. Sheng, S. Wang, and J. Zhang, *Phys. Plasmas* **24**, 102101 (2017).
- ¹²D. Biskamp, in *Magnetic Reconnection in Plasmas*, edited by M. G. Haines and K. I. Hopcraft (Cambridge University Press, Cambridge, 2000).
- ¹³J. Birn, J. F. Drake, M. A. Shay, B. N. Roger, R. E. Denton, M. Hesse, M. Kuznetsova, Z. Ma, A. Bhattacharjee, A. Otto, and P. L. Pritchett, *J. Geophys. Res.* **106**, 3715, <https://doi.org/10.1029/1999JA900449> (2001).
- ¹⁴W. Daughton, J. Scudder, and H. Karimabadi, *Phys. Plasmas* **13**, 072101 (2006).
- ¹⁵S. Lu, Q. M. Lu, C. Huang, and S. Wang, *Phys. Plasmas* **20**, 061203 (2013).
- ¹⁶M. Hoshino, T. Mukai, T. Terasawa, and I. Shinohara, *J. Geophys. Res.* **106**, 25979, <https://doi.org/10.1029/2001JA900052> (2001).
- ¹⁷J. F. Drake, M. A. Shay, and W. Thongthai, *Phys. Rev. Lett.* **94**, 095001 (2005).
- ¹⁸X. R. Fu, Q. M. Lu, and S. Wang, *Phys. Plasmas* **13**, 012309 (2006).
- ¹⁹P. L. Pritchett, *J. Geophys. Res.* **111**, A10212, <https://doi.org/10.1029/2006JA011793> (2006).
- ²⁰C. Huang, Q. M. Lu, and S. Wang, *Phys. Plasmas* **17**, 072306 (2010).
- ²¹J. Egedal, W. Daughton, and A. Le, *Nat. Phys.* **8**, 321 (2012).
- ²²R. S. Wang, Q. M. Lu, Y. V. Khotyaintsev, M. Volwerk, A. M. Du, R. Nakamura, W. D. Gonzalez, X. Sun, W. Baumjohann, X. Li, T. L. Zhang, A. N. Fazakerley, C. Huang, and M. Y. Wu, *Geophys. Res. Lett.* **41**, 4851, <https://doi.org/10.1002/2014GL061157> (2014).
- ²³J. F. Drake, M. Swisdak, H. Che, and M. A. Shay, *Nature* **443**, 553 (2006).
- ²⁴H. S. Fu, Y. V. Khotyaintsev, M. André, and A. Vaivads, *Geophys. Res. Lett.* **38**, L16104, <https://doi.org/10.1029/2011GL048528> (2011).
- ²⁵M. Y. Wu, Q. M. Lu, M. Volwerk, Z. Vörös, T. L. Zhang, L. C. Shan, and C. Huang, *J. Geophys. Res.* **118**, 4804, <https://doi.org/10.1002/jgra.50456> (2013).
- ²⁶M. Y. Wu, C. Huang, Q. M. Lu, M. Volwerk, R. Nakamura, Z. Vörös, T. L. Zhang, and S. Wang, *J. Geophys. Res.* **120**, 6320, <https://doi.org/10.1002/2015JA021165> (2015).
- ²⁷C. Huang, M. Y. Wu, Q. M. Lu, R. S. Wang, and S. Wang, *J. Geophys. Res.* **120**, 1759, <https://doi.org/10.1002/2014JA020918> (2015).
- ²⁸S. Lu, V. Angelopoulos, and H. S. Fu, *J. Geophys. Res.* **121**, 9483, <https://doi.org/10.1002/2016JA022815> (2016).
- ²⁹P. L. Pritchett, *Phys. Plasmas* **15**, 102105 (2008).
- ³⁰M. Oka, T. D. Phan, S. Krucher, M. Fujimoto, and I. Shinohara, *Astrophys. J.* **714**, 915 (2010).
- ³¹K. G. Tanaka, T. Yumura, M. Fujimoto, I. Shinohara, S. V. Badman, and A. Grocott, *Phys. Plasmas* **17**, 102902 (2010).
- ³²G. P. Zank, J. A. le Roux, G. M. Webb, A. Dosch, and O. Khabarova, *Astrophys. J.* **797**, 28 (2014).
- ³³J. T. Dahlin, J. F. Drake, and M. Swisdak, *Phys. Plasmas* **21**, 092304 (2014).
- ³⁴J. T. Dahlin, J. F. Drake, and M. Swisdak, *Phys. Plasmas* **22**, 100704 (2015).
- ³⁵J. T. Dahlin, J. F. Drake, and M. Swisdak, *Phys. Plasmas* **23**, 120704 (2016).
- ³⁶J. T. Dahlin, J. F. Drake, and M. Swisdak, *Phys. Plasmas* **24**, 092110 (2017).
- ³⁷X. C. Li, F. Guo, H. Li, and G. Li, *Astrophys. J. Lett.* **811**, L24 (2015).
- ³⁸X. C. Li, F. Guo, H. Li, and G. Li, *Astrophys. J.* **843**, 21 (2017).
- ³⁹H. Y. Wang, Q. M. Lu, C. Huang, and S. Wang, *Astrophys. J.* **821**, 84 (2016).
- ⁴⁰H. Y. Wang, Q. M. Lu, C. Huang, and S. Wang, *Phys. Plasmas* **24**, 052113 (2017).
- ⁴¹G. D. Holman, L. H. Sui, R. A. Schwartz, and A. G. Emslie, *Astrophys. J. Lett.* **595**, L97 (2003).
- ⁴²V. M. Vasiliunas, *J. Geophys. Res.* **73**, 2839, <https://doi.org/10.1029/JA073i009p02839> (1968).
- ⁴³M. Maksimovic, V. Pierrard, and J. F. Lemaire, *Astro. Astrophys.* **324**, 725 (1997).
- ⁴⁴Q. M. Lu, L. C. Shan, C. L. Shen, T. L. Zhang, Y. R. Li, and S. Wang, *J. Geophys. Res.* **116**, A03224, <http://doi.org/10.1029/2010JA016118> (2011).
- ⁴⁵T. Northrop, 1963, *The Adiabatic Motion of Charged Particles* (Wiley, New York, 1963).